Plasma-catalytic hydrogenation of CO_2 for the cogeneration of CO and CH_4 in a dielectric barrier discharge reactor: Effect of argon addition

Yuxuan Zeng and Xin Tu*

Department of Electrical Engineering and Electronics, University of Liverpool, Liverpool, L69 3GJ, UK

***Corresponding author**

Dr. Xin Tu

Department of Electrical Engineering and Electronics,

University of Liverpool

Liverpool, L69 3GJ

UK

E-mail: xin.tu@liverpool.ac.uk

Tel: +44-1517944513

Abstract

Plasma-catalytic CO_2 hydrogenation over a Ni/Al_2O_3 catalyst for the cogeneration of CO and CH_4 has been carried out in a dielectric barrier discharge (DBD) reactor at 150 ^oC. The presence of the Ni catalyst in the DBD reactor has clearly demonstrated a plasma-catalytic synergistic effect at low temperatures, as the reaction performance of the plasma-catalytic CO_2 hydrogenation is significantly higher than that of the sum of the individual processes (plasma process and thermal catalytic process) at the same temperature. The addition of argon (up to 60%) in the reaction enhances the conversion of CO_2, the yield of CO and CH_4 and the energy efficiency of the plasma process. The formation of metastable argon (Ar*) in the plasma could create new reaction routes which make a significant contribution to the enhanced CO_2 conversion and production of CO and CH_4. The introduction of Ar decreases the breakdown voltage of the feed gas and promotes charge transfer through the reactor. In addition, we find that the selectivity of CO is almost independent of the Ar content in the feed gas, while increasing the Ar content from 0 to 60% enhances the CH_4 selectivity by 85%. This phenomenon suggests that the presence of Ar* might promote the methanation of CO and CO_2 with hydrogen at low temperatures. Moreover, the molar ratio of CO/CH_4 in the plasma-catalytic hydrogenation of CO_2 can also be controlled by changing the Ar content in the feed gas.

Keywords: dielectric barrier discharge, plasma-catalysis, CO_2 hydrogenation, CO_2 methanation, dielectric constant

1. Introduction

CO_2 is one of the major contributors to the global greenhouse gas effect and climate change. The concentration of CO_2 in the atmosphere is continuously increasing due to the use of fossil fuels. There is a growing and urgent demand for the development of novel technologies which can significantly reduce global CO_2 emissions whilst generating sustainable energy for modern society [1-2]. The UK government has set a target to reduce its greenhouse gas emissions by 80% from 1990 levels by 2050, with an interim target of 34% reduction by 2020. The direct use of CO_2 for the production of value-added fuels and chemicals after the CO_2 capture process, or even without capture, has been considered as a promising process to tackle the current global energy and environmental challenges [3]. CO_2 hydrogenation with H_2 for the production of CH_4 (R1) and/or CO_2 (R2) is an attractive approach for direct CO_2 conversion and utilisation (CCU). CH_4 is a fuel and commodity gas, while CO is an important chemical feedstock for Fischer-Tropsch synthesis (FTS) to produce higher hydrocarbons such as liquefied petroleum gas (LPG), naphtha, gasoline, and diesel; or for the synthesis of valorised products such as acetic acid, phosgene, and formic acid [4-6]. If the required energy for these processes can be supplied from renewable energy sources such as wind or solar power, and hydrogen can also be renewable such as from water electrolysis, solar thermal water splitting, or bioenergy [7-8], the overall CCU process could be CO_2 neutral and eco-friendly. Clearly, this process can also be considered as a key approach for chemical energy storage [9].

$$CO_2 + 4H_2 \rightarrow CH_4 + 2H_2O, \qquad \Delta H_r^0 = -163.5 \text{ kJ mol}^{-1} \qquad \text{(R1)}$$

$$CO_2 + H_2 \rightarrow CO + H_2O, \qquad \Delta H_r^0 = 41.2 \text{ kJ mol}^{-1} \qquad \text{(R2)}$$

Since CO_2 is highly stable, the activation of CO_2 molecules requires a high energy input. For example, the thermodynamic equilibrium calculation for the decomposition of pure CO_2 shows that CO_2 begins to decompose into CO and O_2 near 2000 K with a very low conversion (<1%). A higher temperature (3000-3500 K) is required to achieve a reasonable conversion of CO_2 (30–60%). In addition, separation of CO and O_2 in the direct CO_2 decomposition process is also a challenge. Great efforts have been devoted to the investigation of CO_2 hydrogenation into CO and/or CH_4 using thermal catalytic [10-14], photocatalytic [15-16] or electrochemical [17-18] processes. However, significant fundamental works are still required to further enhance the overall energy efficiency and product selectivity of the process through the design and development of new reactor concepts and novel catalytic materials with higher reactivity and stability.

Non-thermal plasma (NTP) provides a promising alternative to the conventional catalytic approach for CO_2 conversion and utilisation at atmospheric pressure and low temperatures. NTP could dissociate and activate gaseous species to produce a cascade of highly reactive species and energetic electrons at ambient conditions, providing alternative reaction pathways, kinetically initiating and propagating thermodynamically unfavourable reactions at low temperatures [19]. The non-thermal plasma chemical process can be switched on and ~~switched~~ off quickly due to its instant reaction initiation with high reaction rate and has great potential to be combined with renewable energy sources, especially waste energy from wind or solar power for localised or distributed chemical energy storage.

NTP is also highly flexible in that it can be combined with other technologies such as catalysis, forming a hybrid plasma-catalytic process. The combination of plasma and catalyst can reduce the activation barrier of catalysts and enhance the reaction

performance, especially the selectivity of target products and energy efficiency of the overall plasma-catalytic process [20]. In the past few years, significant efforts have been dedicated to understanding the plasma conversion of CO_2 into CO [21-27] and dry CO_2 reforming of CH_4 [28-31], with or without ~~using~~ catalysts. However, very limited work has focused on plasma CO_2 hydrogenation for the production of CO and/or CH_4 at low temperatures. Interestingly, in either direct CO_2 splitting or CO_2 dry reforming processes based on NTP technology, the presence of dilution gas (e.g. He and Ar) has shown the positive effect of enhancing the conversion of reactants [10, 32]. However, such a process can only be attractive when the injected dilution gas can be recycled to form a chemical looping process due to the cost of these gases. It is also interesting to investigate how the presence of these gases affects the characteristics of the plasma and consequently changes the reaction performance. To the best of our knowledge, very limited work has been focused on the investigation of how the dilution gases (e.g. Ar) affect the plasma-catalytic chemical reactions especially CO_2 hydrogenation for the synthesis of fuels and chemicals such as the cogeneration of CO and CH_4.

In this work, hydrogenation of CO_2 for the cogeneration of CO and CH_4 has been carried out in a coaxial dielectric barrier discharge (DBD) reactor with and without a Ni/Al_2O_3 catalyst at atmospheric pressure and low temperature (150 ^oC). To understand the synergistic effect of plasma-catalysis, thermal catalytic hydrogenation of CO_2 has also been performed at the same temperature (150 ^oC) for comparison. The effect of Ar as a dilution gas on the CO_2 hydrogenation process under three different operating conditions (plasma only, plasma-catalysis and thermal catalysis) has been investigated in terms of the conversion of CO_2, the selectivity and yield of target products (CO and CH_4), and the fuel production efficiency of the process. The

promotional effect of Ar on the electrical properties of the DBD and the synergistic effect of plasma-catalysis are also discussed.

2. Experimental setup

2.1. Experimental system

Figure 1 shows a schematic diagram of the system set-up. The experiments were carried out in a coaxial packed-bed DBD reactor. A quartz tube with an outer diameter of 21 mm and a wall thickness of 2.5 mm was used as a dielectric layer. A stainless steel mesh wrapped around the quartz tube served as a ground electrode, while a stainless steel rod with a diameter of 13 mm was used as a high voltage electrode and placed in the center of the quartz. The discharge length was 100 mm with a discharge gap of 1.5 mm. The DBD reactor was connected to a high voltage AC power supply with a maximum peak voltage of 30 kV. The voltage on the external capacitor (C_{ext} = 0.47 μF) was measured to obtain the total charge (Q_{ext}) generated in the plasma reaction, while the applied voltage was measured by a high voltage probe (Testec, HVP-15HF). Both signals were recorded by a digital oscilloscope (Tektronix MDO3014). The discharge power was determined by calculating the area of the Q-U Lissajous figure. A homemade power measurement system was used to monitor and control the discharge power in real time. In this work, the discharge power was fixed at 30 W.

A reactant mixture of H_2 and CO_2 with a H_2/CO_2 molar ratio of 4:1 was used and the Ar concentration was varied to 0, 30, 50 and 60%. The total gas flow rate was 69.2 ml min^{-1}. 15 wt.% Ni/γ-Al_2O_3 catalyst was prepared by impregnation method using nitrate salt (Alfa Aesar, ACS reagents) as the metal precursor. Catalyst support (γ-Al_2O_3 beads with a diameter of around 1.5 mm) was added to the solution of nitrate

salt. The mixture slurry was continuously stirred for 1 h and impregnated for 3 h, then dried at 90 ℃ overnight, followed by calcination at 400 ℃ for 4 h. A total of 0.4 g Ni catalyst was packed into the reactor and sandwiched by 2 g Al_2O_3 beads, as shown in figure 1. Prior to the plasma- catalytic CO_2 hydrogenation, the Ni catalyst was reduced in an argon-hydrogen discharge at a discharge power of 30 W (69.2 ml min^{-1}, 20 vol. % H_2) for 30 minutes in the same reactor.

The DBD reactor was placed in a tube furnace, which enabled the CO_2 hydrogenation reaction to be investigated under three different conditions: plasma alone, thermal catalysis and plasma-catalysis. Under plasma alone conditions, no catalyst or alumina bead was placed in the reactor and the reaction was only driven by the plasma. In thermal catalytic reaction, Ni/Al_2O_3 catalyst and alumina beads were packed into the middle of the reactor and heated in the tube furnace without plasma. In the plasma-catalytic process, the Ni catalyst and alumina beads were placed in the DBD plasma with interactions between the plasma and catalyst. The temperature of the reactor was kept at 150 ^oC for all three conditions, monitored by a thermocouple attached to the outer surface of the quartz tube. However, only for the thermal-catalytic process was the reactor heated by the tube furnace, while no extra heating was provided to the plasma process with or without a catalyst.

The gas composition was analysed by a two-channel gas chromatograph (Shimadzu GC-2014) equipped with a flame ionization detector (FID) and a thermal conductivity detector (TCD). For each measurement, three samples of gas products were taken and analysed when the reaction reached a steady state. CO and CH_4 were the major gas products in the plasma hydrogenation of CO_2, while trace amount of saturated hydrocarbons C_2H_6 (40-110 ppm), C_3H_8 (2-20 ppm) and C_4H_{10} (2-20 ppm) were also detected.

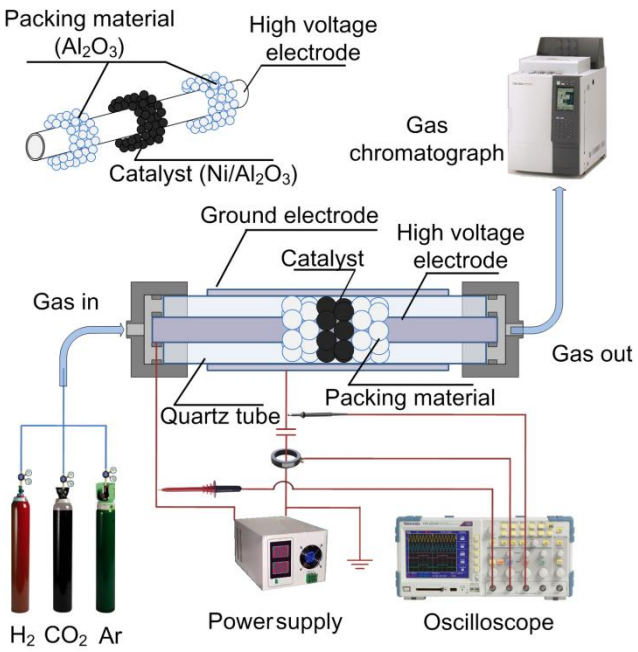

Figure 1. Schematic diagram of experimental setup.

2.2. Definition of parameters

An equivalent circuit developed from our previous work is used to simplify and describe the DBD system in this work [33]. As shown in figure 2, l_{total} is the length (100 mm) of the discharge area and l_{cat} is the actual length of the catalyst bed containing gas, while l_{bed} is the actual length (60 mm) of the packed bed, consisting of the Ni catalysts (black sphere), alumina beads (white sphere), and the gas in the bed. Ideally, if we consider the solid (packing material) and gas in the packed bed separately, we can introduce two equivalent parameters $l_{packing}$ and $l_{gas,2}$. $l_{packing}$ represents the equivalent length of the packed materials (Ni/Al_2O_3 catalyst and Al_2O_3 beads) excluding gas, while $l_{gas,2}$ is the equivalent length of the gas in the packed bed. $l_{gas,1}$ is used to describe the equivalent length of the gas outside of the packing bed.

The equivalent capacitance (before breakdown) of these parameters is denoted as $C_{packing}$, $C_{gas,2}$, and $C_{gas,1}$, respectively, as shown in figure 2. The capacitance of the

quartz barrier is denoted as C_{quartz}. U_b is the breakdown voltage of the gas in the reactor, while the bidirectional diode represents the breakdown and discharge in the reactor. Since the diameter of Al_2O_3 beads is the same as the discharge gap (1.5 mm), we assume that there was only one layer of packing materials (Ni catalyst and Al_2O_3) in the gap when they were tightly packed. In this circumstance, this configuration can be considered as a two-dimensional analogue of the Kepler conjecture and the fraction β of the volume packed with the Ni catalyst and Al_2O_3 beads is about 0.9 [34]. The relationship of these parameters is summarised below.

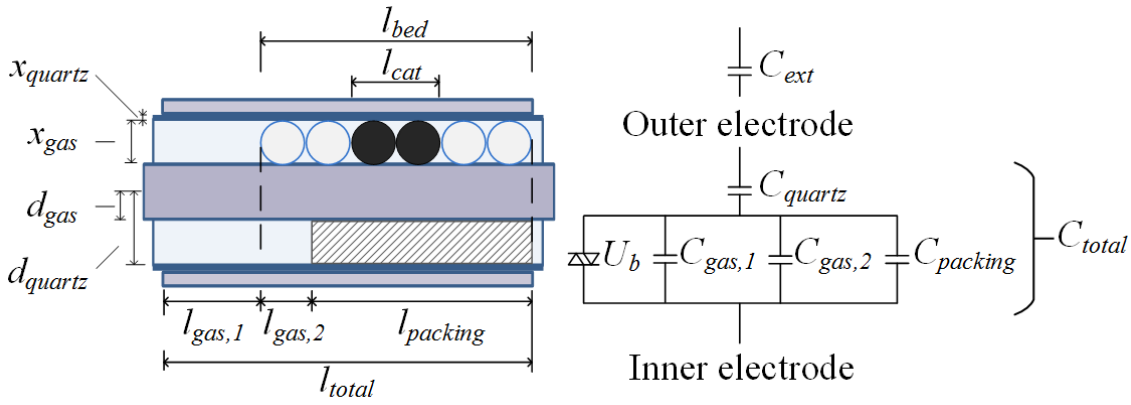

Figure 2. Equivalent circuit of the DBD-catalytic reactor.

$$l_{packing} = l_{bed} \times \beta \qquad \text{(Eq 1)}$$

$$l_{gas,2} = l_{bed} - l_{packing} = l_{total} - l_{packing} - l_{gas,1} \qquad \text{(Eq 2)}$$

The values of the capacitances fit the following equations.

$$\frac{1}{C_{total}} = \frac{1}{C_{quartz}} + \frac{1}{C_{gap}} = \frac{1}{C_{quartz}} + \frac{1}{(C_{gas,1}+C_{gas,2}+C_{packing})} \qquad \text{(Eq 3)}$$

where C_{total} is the total capacitance of the reactor packed with catalysts and Al_2O_3,

C_{gap} is the overall capacitance of the gap. Both parameters were calculated from the Lissajous figure [35]. $C_{gas,1}$, $C_{gas,2}$, and C_{quartz} were calculated from the following equation of cylindrical capacitors [36]:

$$C_i = \frac{2\pi\varepsilon_0\varepsilon_i l_i}{ln(d_i+x_i) - ln\, d_i} \quad \text{(Eq 4)}$$

where ε_0 is the dielectric constant of vacuum (8.85×10^{-12} F m^{-1}). ε_i, l_i, d_i, and x_i are the relative dielectric constant, the (equivalent) length, the inner radius, and thickness of the corresponding material (figure 2), respectively. Here ε_{quartz} is 4.65 [37], while ε_{gas} is 1 because the relative dielectric constants of Ar, H_2 and CO_2 are close to unity [38-40]. The overall relative dielectric constant of the packing material (Ni/Al_2O_3 and Al_2O_3 beads) $\varepsilon_{packing}$ is unknown, because the Ni particles supported on Al_2O_3 have changed its surface properties. However this parameter can be determined *via* $C_{packing}$ and Lissajous figure.

As explained in our previous work [33], the charge transferred through the reactor (Q_{pp}) can be measured by the capacitor C_{ext}, while the charge transferred during the discharge (Q_d) and the charge transferred from one electrode to the other (Q_{trans}) can be calculated *via* the Lissajous figure. The voltage applied on the reactor, the discharge gap, the quartz wall, two parts of gas in the gap namely $l_{gas,1}$ and $l_{gas,2}$, are presented as U, U_{gap} , U_{quartz}, $U_{gas,1}$, and $U_{gas,2}$, respectively. Thus, we have:

$$U_{gap} = U_{gas,1} = U_{gas,2} \quad \text{(Eq 5)}$$

$$U_{gap} = U - U_{quartz} = U - \frac{C_{ext}U_{ext}}{C_{quartz}} \quad \text{(Eq 6)}$$

where U_{ext} is the voltage across the external capacitor.

For the plasma-catalytic CO_2 hydrogenation, the conversion (X) of CO_2 is defined

as:

$$X_{CO2}\ (\%) = \frac{\mathrm{CO_2\ converted\ (mol)}}{\mathrm{CO_2\ input\ (mol)}} \times 100 \qquad \text{(Eq 7)}$$

The selectivity (*S*) and yield (*Y*) of the main products are calculated as:

$$S_{CO}\ (\%) = \frac{\mathrm{CO\ produced\ (mol)}}{\mathrm{CO_2\ converted\ (mol)}} \times 100 \qquad \text{(Eq 8)}$$

$$S_{CH4}\ (\%) = \frac{\mathrm{CH_4\ produced\ (mol)}}{\mathrm{CO_2\ converted\ (mol)}} \times 100 \qquad \text{(Eq 9)}$$

$$Y_{CO}\ (\%) = \frac{\mathrm{CO\ produced\ (mol)}}{\mathrm{CO_2\ input\ (mol)}} \times 100 \qquad \text{(Eq 10)}$$

$$Y_{CH4}\ (\%) = \frac{\mathrm{CH_4\ produced\ (mol)}}{\mathrm{CO_2\ input\ (mol)}} \times 100 \qquad \text{(Eq 11)}$$

The H_2/CO_2 molar ratio and carbon balance (*B*) are determined as follows:

$$\frac{\mathrm{H_2}}{\mathrm{CO_2}} = \frac{\mathrm{H_2\ input\ (mol)}}{\mathrm{CO_2\ input\ (mol)}} \qquad \text{(Eq 12)}$$

$$B_{carbon}\ (\%) = \frac{[\mathrm{CH_4}]_{out} + [\mathrm{CO_2}]_{out} + [\mathrm{CO}]_{out}}{[\mathrm{CO_2}]_{in}} \times 100 \qquad \text{(Eq 13)}$$

The fuel production efficiency (*FPE*) of the process is determined as follows:

$$FPE\ (\%) = \frac{\mathrm{LHV_{CO}\ (J\ mol^{-1})} \times \mathrm{CO\ output\ (mol\ s^{-1})} + \mathrm{LHV_{CH4}\ (J\ mol^{-1})} \times \mathrm{CH_4\ output\ (mol\ s^{-1})}}{\mathrm{LHV_{H2}\ (J\ mol^{-1})} \times \mathrm{H_2\ input\ (mol\ s^{-1})} + \mathrm{discharge\ power\ (W)}} \times 10 \qquad \text{(Eq 14)}$$

where LHV is the lower heating value of fuels. The synergistic capability of plasma catalysis in percentage (*SC*) is calculated as [41]:

$$SC_{\zeta}\ (\%) = \frac{\zeta_{p+c} - \zeta_p - \zeta_c}{\zeta_p + \zeta_c} \times 100 \qquad \text{(Eq 15)}$$

where ζ can be the conversion of CO_2, the yield of CO, the selectivity and yield

of CH_4, or the fuel production efficiency. The subscripts *p+c*, *p*, and *c* represent the results from plasma-catalysis, plasma alone, and thermal catalysis (catalyst only), respectively.

3. Results and discussion

3.1. Effect of Ar on CO_2 hydrogenation

Figure 3 shows the influence of argon content on the conversion of CO_2 at the same temperature of 150 ^oC under different process conditions. Without using plasma, it is almost impossible to convert CO_2 or H_2 at such a low temperature in the catalytic hydrogeneration of CO_2 (R3 and R4) [42-43]. In the plasma process without a catalyst, the conversion of CO_2 significantly increases from 18.3% to 38.0% when increasing the Ar content from 0 to 60%. Similarly, in the plasma-catalytic hydrogeneration of CO_2, the CO_2 conversion is almost doubled (from 29.1% to 56.1%) when increasing the Ar content from 0 to 60%, while the carbon balance remains constant at 99%. Clearly, the presence of Ar in the plasma process has a positive effect on the conversion of CO_2.

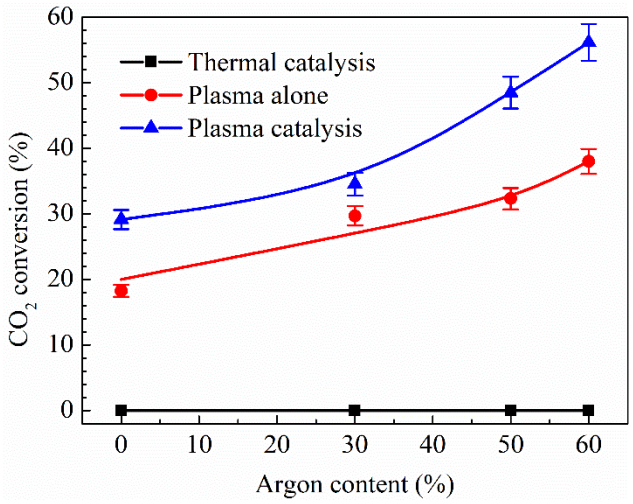

Figure 3. Effect of Ar content on CO_2 conversion using different process conditions

at 150 ^{o}C. (H_2/CO_2 = 4: 1, total flow rate 69.2 ml min^{-1}, discharge power of DBD 30 W).

The addition of Ar in the mixture gas (CO_2 + H_2) increases the average first townsend ionisation coefficient of the feed gas, which makes the discharge form more easily. Ramakers *et al.* [44] calculated the electron density, mean electron energy, and rate constant relating to the dissociation of CO_2 in a DBD plasma. They found that all these values increased when adding Ar in the CO_2 DBD. The ionisation of Ar requires a much higher electron energy (15.76 eV) than that for the excitation of Ar such as 11.55 eV for Ar ($4s^3P_2$), and 11.72 eV for Ar ($4s'^3P_0$) [45]. Thus, Ar is more likely excited to its metstable state (R5) rather than being ionised. The presense of metastable Ar species (Ar*) could create new reaction pathways for the dissociation of CO_2 and H_2 in the plasma hydrogenation of CO_2, as shown in reaction R6 and R7 [45-47]. All these effects contribute to the enhanced conversion of H_2 and CO_2 when increasing the Ar content in the $Ar/CO_2/H_2$ DBD.

$$e^- + CO_2 \rightarrow CO + O + e^- \quad \text{(R3)}$$

$$e^- + H_2 \rightarrow H + H + e^- \quad \text{(R4)}$$

$$e^- + Ar \rightarrow e^- + Ar^* \quad \text{(R5)}$$

$$Ar^* + CO_2 \rightarrow CO + O + Ar \quad \text{(R6)}$$

$$Ar^* + H_2 \rightarrow H + H + Ar \quad \text{(R7)}$$

In addition, compared to the plasma reaction without a catalyst, the combination of the plasma with the Ni catalyst significantly enhances the conversion of CO_2 by 16%–60%. Increasing the Ar content in the feed also enhances the conversion of CO_2. The presence of Ar in the CO_2 DBD leads to a more uniform discharge, which might increase the contact area between the plasma and catalyst and consequently enhance

the plasma-catalyst interactions and plasma-assisted surface reactions. It is also worth noting that the CO_2 conversion in the plasma-catalytic hydrogenation of CO_2 is always higher than the sum of the CO_2 conversion in the plasma reaction without a catalyst and that of the thermal-catalytic reaction at the same temperature. These results clearly show a low temperature synergistic effect of plasma-catalysis, resulting from the interactions between the plasma and Ni/Al_2O_3 catalyst in the plasma-catalytic reaction.

The selectivity and yield of CO and CH_4 under different conditions are shown in figure 4. Neither CO nor CH_4 is detected in the thermal catalytic hydrogeneration of CO_2 at 150 ^oC, due to the very low conversion of CO_2 at such a low temperature. In the plasma reaction without a catalyst, increasing the Ar content from 0 to 60% significantly enhances the selectivity of CH_4 by 85%. By contrast, the selectivity of CO is almost constant when changing the Ar concentration. This phenomenon suggests that the presence of Ar* in the reaction might create new reaction routes for the formation of CH_4, resulting in the enhanced CH_4 selectivity and slightly decreased CO selectivity when increasing the Ar content.

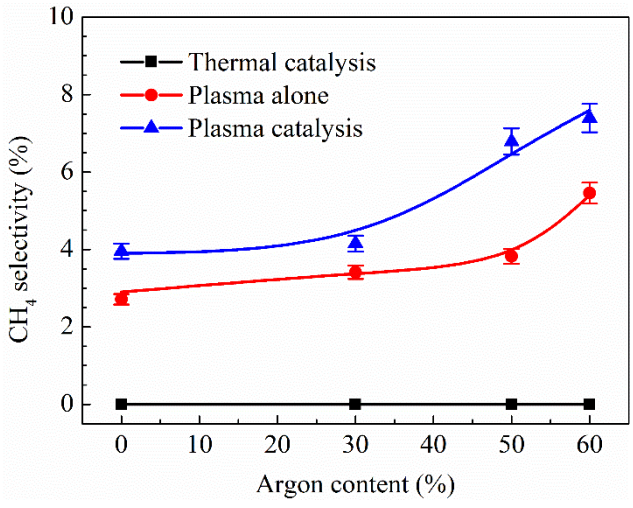

(a)

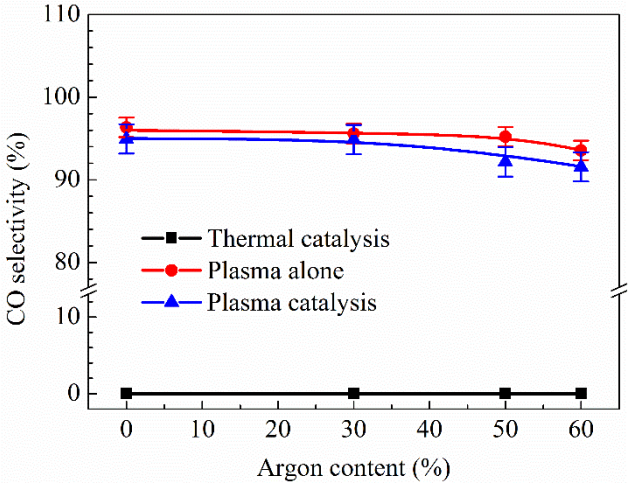

(b)

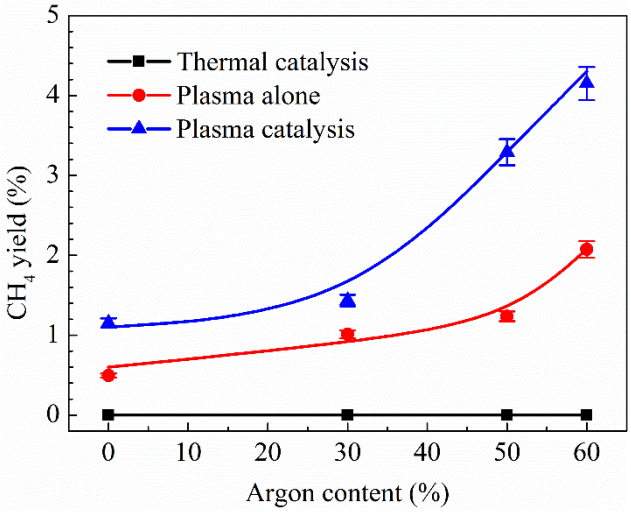

(c)

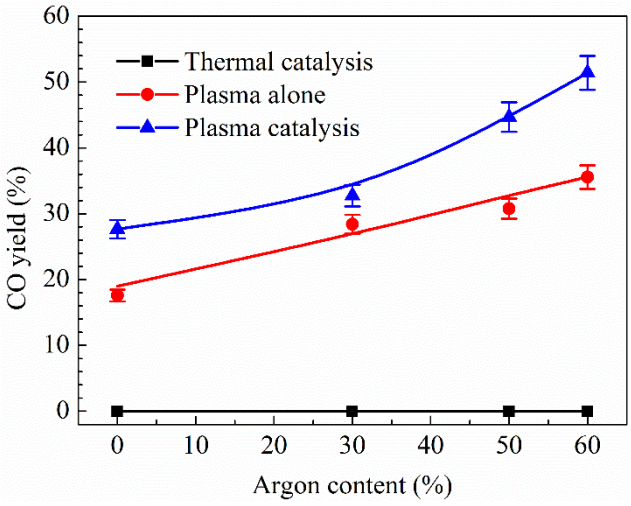

(d)

Figure 4. Effect of Ar content on: (a) CH_4 selectivity; (b) CO selectivity; (c) CH_4

yield and (d) CO yield in the hydrogenation of CO_2 at 150 ^oC. (H_2/CO_2 = 4: 1, total flow rate 69.2 ml min^{-1}, discharge power of plasma 30 W).

To understand the reaction pathways for the formation of CH_4 in the plasma hydrogenation of CO_2, we have developed a zero-dimensional chemical kinetics model to simulate the plasma chemistry in the CO_2/H_2 DBD. In this model, the time evolution of the density of the species is calculated based on the production and loss terms, as defined by the chemical reactions. The electron temperature is calculated with an energy balance equation, while the rate coefficients of the electron impact reactions are calculated in a Boltzmann equation model, as a function of the electron temperature and cross-section of target species [43]. The plasma chemistry used in the model is based on the plasma chemistry set established in the literature [48]. Figure 5 shows the possible major reactions for the formation of CH_4 in the plasma process.

In the plasma hydrogenation of CO_2 without a catalyst, CH_4 is mainly formed from CO as described in reaction R8–R10 [49]. CH has been considered the most important precursor for the formation of CH_4. The plasma modelling shows that CH radicals are mainly generated through the reaction of carbon with H_2 (R11), while carbon could be produced from the dissociation of CO by electrons and Ar* (R13 and R14). The rate coefficient of reaction R12 to form CH_2 directly from carbon and H_2 is significantly lower than that of reaction R11 [50-51]. The reaction of CO with H can produce HCO intermediate (R15) [52]. However, further hydrogenation of HCO can easily happen to produce H_2 and CO [53]. The rate coefficient of this reaction (R16) is similar to that of reaction R15. The formation of CH from CHO is very difficult in the gas-phase reaction.

The selectivity of CH_4 is significantly lower than the CO selectivity as the dissociation of CO to form carbon is weak. In addition, no carbon deposition is

observed in the DBD reactor as the formed carbon can react with H_2 to form CH_x species due to the high H_2/CO_2 ratio. The presence of Ar* could also contribute to the dissociation of CO to generate carbon (R14), which might explain the enhanced CH_4 formation with a higher Ar content in the reactants.

$CH + H_2 \rightarrow CH_2 + H$ (R8)

$CH_2 + H_2 \rightarrow CH_3 + H$ (R9)

$CH_3 + H + M \rightarrow CH_4 + M$ (R10)

$C + H_2 \rightarrow CH + H$ (R11)

$C + H_2 \rightarrow CH_2$ (R12)

$e^- + CO \rightarrow C + O + e^-$ (R13)

$Ar^* + CO \rightarrow C + O + Ar$ (R14)

$H + CO + M \rightarrow HCO + M$ (R15)

$HCO + H \rightarrow H_2 + CO$ (R16)

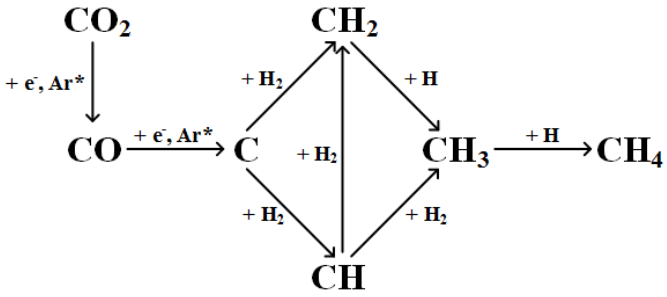

Figure 5. Major reaction pathways of CH_4 formation in the plasma hydrogenation of CO_2

Compared with the plasma hydrogenation of CO_2 without a catalyst, the coupling of DBD plasma with the Ni/Al_2O_3 catalyst further enhances the selectivity of CH_4 due to the creation of new reaction routes over the surface of the Ni/Al_2O_3 catalyst. A

synergistic effect between the plasma and catalyst on the selectivity of CH_4 can be clearly identified. The selectivity of CH_4 in the plasma-catalytic CO_2 hydrogenation (S_{p+c}) is always larger than the sum of the CH_4 selectivity in the plasma-alone and catalysis-alone processes ($S_{p+c} > S_p + S_c$). However, the presence of the Ni/Al_2O_3 catalyst in the plasma-hydrogenation of CO_2 has a weak effect on the selectivity of CO. The reaction mechanisms proposed for catalytic CO_2 methanation over a Ni catalyst involve the conversion of CO_2 to CO, and subsequent reactions following the same mechanism as CO methanation [24]. In the plasma-catalytic CO_2 hydrogenation, the adsorbed CO can originate from the plasma dissociation of CO_2 in the gas phase (R3) [42] or the dissociation of adsorbed CO_2 on the catalyst surface (R17 and R18) [54-55]. It has been proposed that CH_4 can be formed from the formation of the CHO intermediate (R19) and its hydrogenation (R20, R24 and R25) [56], or the formation of surface carbon in CO dissociation (R21 and R22) and its interaction with hydrogen (R23–R25) [24, 54].

$$CO + M \rightarrow CO_{ads} \quad \text{(R17)}$$

$$CO_{2,\,ads} \rightarrow CO_{ads} + O_{ads} \quad \text{(R18)}$$

$$CO_{ads} + H_{ads} \rightarrow CHO_{ads} \quad \text{(R19)}$$

$$CHO_{ads} \rightarrow CH_{ads} + O_{ads} \quad \text{(R20)}$$

$$CO_{ads} \rightarrow C_{ads} + O_{ads} \quad \text{(R21)}$$

$$2\,CO_{ads} \rightarrow C_{ads} + CO_{2,\,ads} \quad \text{(R22)}$$

$$C_{ads} + H_{ads} \rightarrow CH_{ads} \quad \text{(R23)}$$

$$CH_{ads} + H_{ads} \rightarrow CH_{2,\,ads} \quad \text{(R24)}$$

$$CH_{2,\,ads} + 2\,H_{ads} \rightarrow CH_4 \quad \text{(R25)}$$

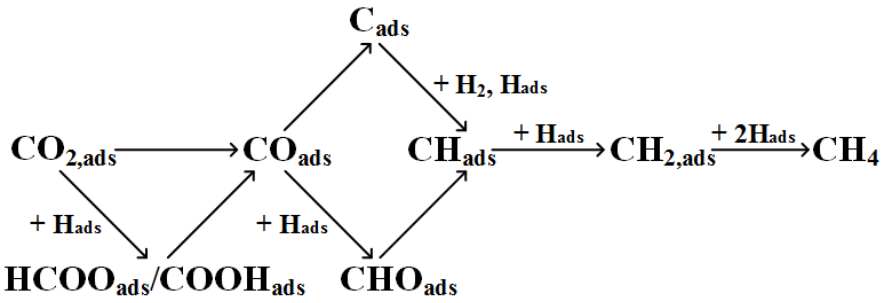

Figure 6. Possible major reactions for the formation of CH_4 on the Ni/Al_2O_3 catalyst

The yield of CH_4 and CO increases with the Ar content in the plasma process with or without the Ni/Al_2O_3 catalyst. For instance, increasing the Ar content from 0 to 60% significantly enhances the CH_4 yield by 250% in the plasma-catalytic process, while the CO yield is only increased by 85.6%. Placing the Ni/Al_2O_3 catalyst in the DBD also enhances the yield of CH_4 and CO compared with the plasma reaction in the absence of the Ni catalyst. A significant synergistic effect between the plasma and the Ni catalyst on the yield of CH_4 and CO can be clearly identified in figure 4.

Figure 7 shows the influence of changing the Ar content on the yield of CO and CH_4, and the CO/CH_4 molar ratio in the product during the plasma-catalytic CO_2 hydrogenation. The yield of CH_4 changes more quickly than that of CO when increasing the Ar content up to 60%. Thus, raising the Ar content from 0 to 60% significantly reduces the CO/CH_4 molar ratio from 24 to 12. As we know, using different catalysts can control the selectivity of target products and change the distribution of different products in a chemical reaction. This interesting phenomenon suggests that the molar ratio of CO/CH_4 in the plasma-catalytic hydrogenation of CO_2 can also be controlled by changing the Ar content.

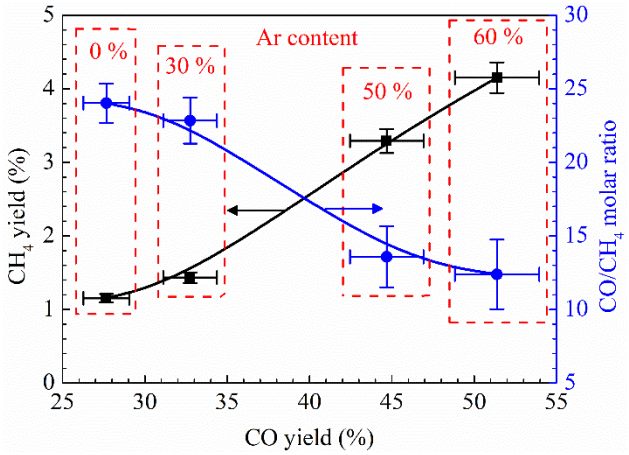

Figure 7. Effect of Ar content on the yield of gas products (CO/CH_4) and CO/CH_4 molar ratio in the plasma-catalytic CO_2 hydrogenation process (H_2/CO_2 = 4: 1, total flow rate 69.2 ml min^{-1}, discharge power of plasma 30 W).

Figure 8 compares the fuel production efficiency of CO_2 hydrogenation under different process conditions. Clearly, the combination of the DBD with the Ni catalyst shows a higher fuel production efficiency due to the plasma-catalytic synergy. In the plasma-catalytic hydrogenation of CO_2, increasing the Ar content slightly enhances the fuel production efficiency of the process. By contrast, the fuel production efficiency of the plasma reaction without the Ni catalyst reaches a maximum at an Ar content of 30%, then decreases with further increasing of the Ar content. The different evolutions of the fuel production efficiency between the plasma-catalytic process and plasma process when changing the Ar content might be attributed to the following effects. At a higher Ar content (*e.g.* > 30%), some of the input energy might go in to the ionisation of Ar rather than the conversion of CO_2. However, in the plasma-catalytic reaction, higher Ar content leads to a more uniform discharge, which significantly enhances the interactions between the plasma and Ni/Al_2O_3 catalyst and consequently the reaction performance of the plasma-catalytic hydrogenation of CO_2. This effect is predominant over the waste of input energy (due to higher Ar content)

in the plasma-catalytic process.

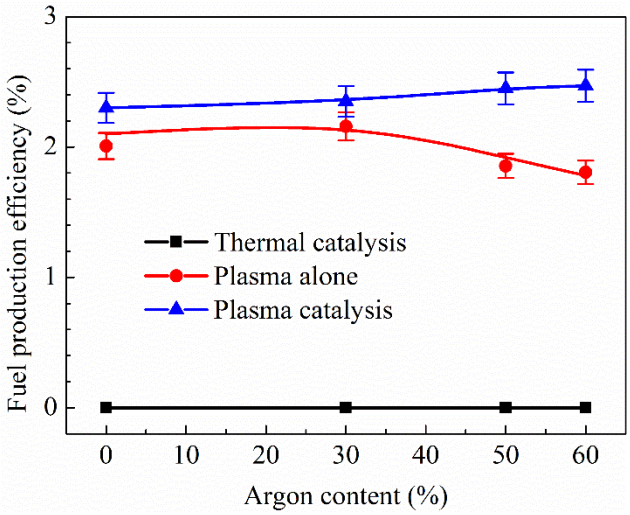

Figure 8. Effect of Ar content on the energy efficiency of CO_2 hydrogenation under different process conditions (H_2/CO_2 = 4: 1, total flow rate 69.2 ml min^{-1}, discharge power of plasma 30 W, temperature 150 ^oC)

3.2. Effect of Ar on the synergistic effect between plasma and catalyst

Synergistic capacity is used to quantify the reaction performance of the plasma-catalytic hydrogenation of CO_2, compared to that using plasma alone or catalyst alone at the same temperature (150 ^oC), as shown in Table 1. The synergy of plasma-catalysis in terms of the conversion of CO_2, the selectivity and yield of CO and CH_4, and the energy efficiency of the process can be clearly seen even without Ar (0%) in the feed gas. For instance, in the plasma-catalytic hydrogenation of CO_2 without Ar, the conversion of CO_2 is 59.6% larger than the sum of the CO_2 conversion using the plasma hydrogenation (without catalyst) and thermal catalysis (without plasma) at the same temperature. The most significant synergy of plasma-catalysis is reflected by the yield of CH_4, which has a synergistic capacity of 132% in the absence of Ar and

reaches a peak value of 166% at an Ar content of 50%. We find the synergistic capacity of the plasma-catalytic process is significantly enhanced when increasing the Ar content from 30% to 60%. As discussed previously, the combination of plasma and Ni catalyst has a more significant effect on the enhanced reaction performance (conversion, selectivity, yield and energy efficiency) compared to the plasma reaction without the Ni/Al_2O_3 catalyst at a higher Ar content (> 30%). Enhanced contact area between the plasma and catalyst and the resulting strong interactions between them when increasing the Ar content from 30 to 60% could be the main driving force for the significant synergistic-capacity of the plasma-catalytic process, although increasing the Ar content wastes energy due to the excitation and ionisation of Ar atoms.

Table 1. Effect of Ar content on the synergistic capacity (*SC*) of the processes. (H_2/CO_2 = 4: 1, total flow rate 69.2 ml min^{-1}, discharge power of plasma 30 W, temperature 150 ^oC)

Ar (%)	SC_C (%)	SC_Y (%)			SC_S (%)	SC_{FPE} (%)
		CH_4	CO	Total		
0	59.6	132	57.3	45.6	59.5	17.1
30	16.2	42	15.3	16.3	21.9	6.5
50	50.0	166	45.2	49.9	77.5	32.2
60	47.7	100	44.5	47.6	35.5	20.8

3.3. Effect of Ar on electrical properties of the DBD

Figure 9 shows the Lissajous figures of the plasma-catalytic CO_2 hydrogenation with

different Ar contents at the same discharge power of 30 W. Although the size of the Lissajous figures change with the Ar content, the gradient of the edges of the parallelograms is maintained when changing the Ar content from 0 to 50%. Various electrical properties of the DBD can be calculated through the Lissajous figure, including C_{total}, C_{eff} (measured from the gradient on the Lissajous figure), U_b, Q_{pp}, Q_d, and Q_{trans}. Theoretically, the effective capacitance C_{eff} is equal to the capacitance of the dielectric material (i.e. C_{quartz}) when the discharge gap is "fully bridged" by the discharge. However, if the gap is not "fully bridged" and fails to transfer all of the charge accumulated on the dielectric material, partial discharging occurs and the value of C_{eff} could be smaller than C_{quartz} [57]. Table 2 shows that the Ar content has a very weak effect on the effective capacitance of the DBD reactor and the properties of charges. However, the calculated C_{eff} (around 139 pF) is lower than the C_{quartz} calculated by equation 4 (154 pF), which suggests the occurrence of partial discharging. The energy-efficiency of the plasma reaction decreases when partial discharging occurs, due to the presence of charge residue on the dielectric layer. As the Ar content increases, the slightly increased effective capacitance of the reactor (C_{eff}) suggests that more power is injected into the plasma for chemical reactions rather than deposited and 'wasted' on the dielectric surface. This finding agrees with the enhanced CO_2 conversion and yield of CH_4 and CO when increasing the Ar content in the reactants. It is difficult to measure the equivalent relative dielectric constant of the packing materials (including the Ni catalyst and pure alumina) $\varepsilon_{packing}$ in a DBD reactor, especially when $\varepsilon_{packing}$ is simultaneously affected by the composition of the catalyst, the loading and redox status of supported metal, and the working status of plasma. However in this work, by solving the formula of C_{total}, C_{quartz}, and C_{gap} in equation 4, the equivalent $\varepsilon_{packing}$ can be estimated as 0.79. This

value is much smaller than the relative dielectric constant of Al_2O_3 (9 to 10), implying that the deposition of Ni particles on the surface of Al_2O_3 beads significantly changes its dielectric constant.

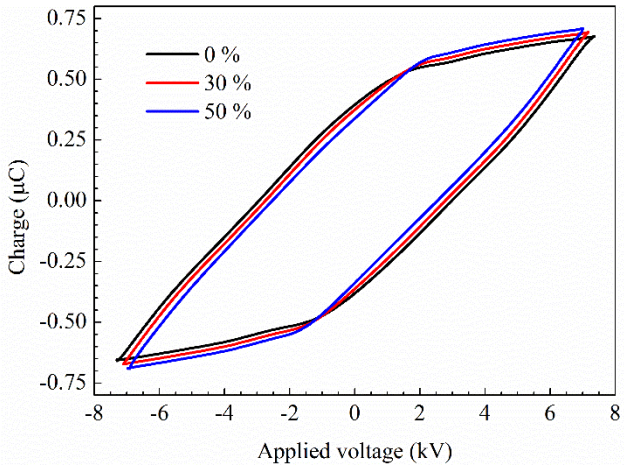

Figure 9. Effect of Ar content on Lissajous figures of the DBD in the plasma-catalytic CO_2 hydrogenation process (H_2/CO_2 = 4: 1, total flow rate 69.2 ml min^{-1}, discharge power of plasma 30 W).

As described previously, Q_{pp}, Q_d, and Q_{trans} evaluate the charge transferred through the DBD reactor during one "discharge off" phase and one "plasma on" phase. A slight increase (~1.5%) is observed for all these parameters when changing the Ar content. The change is almost neglectable, although such phenomenon is reasonable. Since the discharge power is kept at 30 W, increasing the Ar content slightly decreases the applied voltage U_{pp} (figure 10) and accordingly increases the discharge current; thus assisting the charge transfer. The increased discharge current is reflected by the increased Q_d, and the enhanced charge transfer can be evidenced by the enlarged Q_{trans}, as summarised in table 2.

Table 2. Effect of Ar content on the capacitances of the reactor and charges in the

plasma-catalytic CO_2 hydrogenation (H_2/CO_2 = 4: 1, total flow rate 69.2 ml min^{-1}, discharge power of plasma 30 W).

Ar content (%)	C_{eff} (pF)	C_{total} (pF)	Q_{pp} (μC)	Q_d (μC)	Q_{trans} (μC)
0	138.2	27.8	1.35	1.21	0.93
30	139.1	27.2	1.37	1.23	0.99
50	139.4	27.8	1.40	1.25	1.03

Figure 10 shows the effect of the Ar content on the peak-to-peak voltage and breakdown voltage of the DBD in the presence of the Ni catalyst. At a constant discharge power, increasing the Ar content from 0 to 50% slightly decreases the U_{pp} (from 14.7 to 14.1 kV), which suggests that the discharge current would increase with increasing Ar content at a fixed discharge power, and contribute to the enhanced CO_2 conversion at a higher H_2 content. The breakdown voltage U_b also decreased, from 3.1 to 2.6 kV, when increasing the Ar content from 0 to 50%. As mentioned previously, the addition of Ar increases the average first Townsend ionisation coefficient α of the feed gas. Auriemma *et al.* calculated the Townsend coefficient of a gas mixture with various Ar/CO_2 molar ratios. They found that the coefficient of the gas mixture significantly increases with the Ar concentration [42]. In addition, as CO_2 is an electro-negative gas, the introduction of Ar lowers the chance of free electron attachment on CO_2 molecules, facilitating the acceleration of free electrons [44]. Moreover, the increasing amount of Ar decreases the average dielectric strength of the working gas [58]. As a consequence of all these factors, the feed gas between the electrodes would electrically breakdown at a lower voltage U_b, and the DBD plasma would also be sustained at a lower voltage U_{pp}.

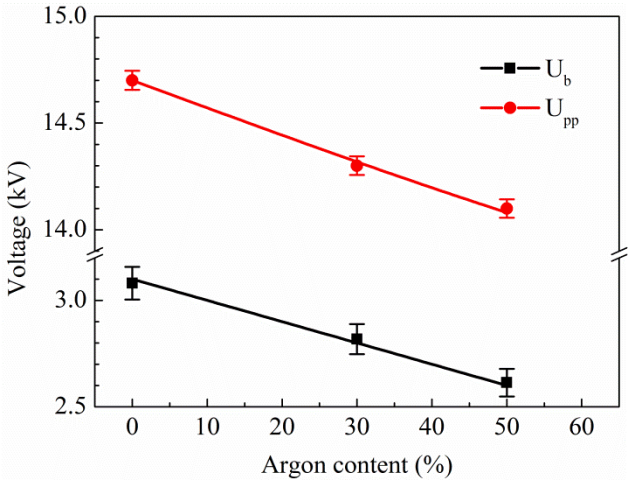

Figure 10. Effect of Ar content on breakdown and peak-to-peak voltages of the DBD in the plasma-catalytic hydrogenation process (H_2/CO_2 = 4: 1, total flow rate 69.2 ml min^{-1}, discharge power of plasma 30 W).

4. Conclusion

Plasma-catalytic CO_2 hydrogenation has been carried out in a DBD reactor at 150 ^oC. The combination of the plasma and Ni/Al_2O_3 catalyst clearly generates a synergistic effect as a result of the interactions between the plasma and catalyst, which enhances the CO_2 conversion, the yield of CO and CH_4 and the energy efficiency of the process compared to the reaction using either plasma alone or the thermal catalytic approach at the same temperature (150 ^oC). In the plasma CO_2 hydrogenation with and without catalyst, the addition of Ar in the feed gas enhances the conversion of CO_2, the selectivity of CH_4, and the fuel production efficiency, while the selectivity of CO is almost independent of the Ar content. The addition of Ar in the feed gas (CO_2/H_2) shifts the discharge mode from “partial discharging” to “fully-bridged” discharge and enhanced the interactions between the DBD and Ni catalyst. The presence of Ar* opens new reaction routes which make a significant contribution to the enhanced

reaction performance. The results show that the molar ratio of CO/CH_4 in the gas product can be adjusted by changing the Ar content in the feed gas. In addition, the presence of Ar in the feed gas changes the electrical properties of the plasma, including decreasing the breakdown voltage and promoting charge transfer through the reactor. The equivalent relative dielectric constant of the packing material (Ni/Al_2O_3 catalyst and Al_2O_3 beads) in the DBD reactor is 0.79, which suggests that loading NiO particles on the surface of alumina changes its electrical properties.

Acknowledgements

The support of this work by the UK EPSRC SUPERGEN Hydrogen & Fuel Cell (H2FC) Hub (EP/J016454/1, Ref EACPR_PS5768) is gratefully acknowledged. Yuxuan Zeng acknowledges the PhD fellowship co-funded by the Doctoral Training Programme (DTP) at the University of Liverpool and the Chinese Scholarship Council (CSC).

References

[1] Bogaerts A, Kozák T, van Laer K and Snoeckx R 2015 *Farad. Discuss.* **183** 217-232

[2] Markewitz P, Kuckshinrichs W, Leitner W, Linssen J, Zapp P, Bongartz R, Schreiber A and Müller T E 2012 *Energy Environ. Sci.* **5** 7281

[3] Song C 2006 *Catal. Today* **115** 2-32

[4] Porosoff M D, Yang X, Boscoboinik J A and Chen J G 2014 *Angew. Chem. Int. Ed.* **53** 6705-6709

[5] Centi G, Quadrelli E A and Perathoner S 2013 *Energy Environ. Sci.* **6** 1711

[6] Ashford B and Tu X 2017 *Current Opinion in Green and Sustainable Chemistry* **3**

45-49

[7] Chueh W C, Falter C, Abbott M, Scipio D, Furler P, Haile S M and Steinfeld A 2010 *Science* **330** 1797-1801

[8] Centi G and Perathoner S 2010 *ChemSusChem* **3** 195-208

[9] Schiermeier Q 2013 *Nature* **496** 156-158

[10] Yan Y, Dai Y, He H, Yu Y and Yang Y 2016 *Appl. Catal., B: Environ.* **196** 108-116

[11] Avanesian T, Gusmão G S and Christopher P 2016 *J. Catal.* **343** 86-96

[12] Heine C, Lechner B A, Bluhm H and Salmeron M 2016 *J. Am. Chem. Soc.* **138** 13246-13252

[13] Zhou G, Liu H, Cui K, Jia A, Hu G, Jiao Z, Liu Y and Zhang X 2016 *Applied Surf. Sci.* **383** 248-252

[14] Gao J, Wu Y, Jia C, Zhong Z, Gao F, Yang Y and Liu B 2016 *Catal. Commun.* **84** 147-150

[15] Puga A V 2016 *Top. Catal.* **59** 1268-1278

[16] Yan Y, Han M, Konkin A, Koppe T, Wang D, Andreu T, Chen G, Vetter U, Morante J R and Schaaf P 2014 *J. Mater. Chem.* **2** 12708-12716

[17] Kalaitzidou I, Makri M, Theleritis D, Katsaounis A and Vayenas C 2016 *Surf. Sci.* **646** 194-203

[18] Jiménez V, Jiménez-Borja C, Sánchez P, Romero A, Papaioannou E I, Theleritis D, Souentie S, Brosda S and Valverde J L 2011 *Appl. Catal., B: Environ.* **107** 210-220

[19] Samukawa S, Hori M, Rauf S, Tachibana K, Bruggeman P, Kroesen G, Whitehead J C, Murphy A B, Gutsol A F, Starikovskaia S, Kortshagen U, Boeuf J-P, Sommerer T J, Kushner M J, Czarnetzki U and Mason N 2012 *J.*

Phys. D: Appl. Phys. **45** 253001

[20] Neyts E C and Bogaerts A 2014 *J. Phys. D: Appl. Phys.* **47** 224010

[21] Bogaerts A, Wang W, Berthelot A and Guerra V 2016 *Plasma Sources Sci. Technol.* **25** 055016

[22] Wang W, Berthelot A, Kolev S, Tu X and Bogaerts A 2016 *Plasma Sources Sci. Technol.* **25** 065012

[23] Lebouvier A, Iwarere S A, d'Argenlieu P, Ramjugernath D and Fulcheri L 2013 *Energy Fuels* **27** 2712-2722

[24] Wang W, Wang S, Ma X and Gong J 2011 *Chem. Soc. Rev.* **40** 3703-3727

[25] Mei D, Zhu X, He Y-L, Yan J D and Tu X 2015 *Plasma Sources Sci. Technol.* **24** 015011

[26] Mei D, Zhu X, Wu C, Ashford B, Williams P T and Tu X 2016 *Appl. Catal., B: Environ.* **182** 525-532

[27] Zeng Y and Tu X 2016 *IEEE Trans. Plasma Sci.* **44** 405-411

[28] Zeng Y X, Zhu X B, Mei D H, Ashford B and Tu X 2015 *Catal. Today* **256** 80-87

[29] Mei D, He Y L, Liu S, Yan J and Tu X 2015 *Plasma Process. Polym.* **13** 544-556

[30] Chung W C and Chang M B 2016 *Renew. Sustainable Energy Rev.* **62** 13-31

[31] Kawi S, Kathiraser Y, Ni J, Oemar U, Li Z and Saw E T 2015 *ChemSusChem* **8** 3556-3575

[32] Kundu S K, Kennedy E M, Gaikwad V V, Molloy T S and Dlugogorski B Z 2012 *Chem. Eng. J.* **180** 178-189

[33] Tu X, Gallon H J, Twigg M V, Gorry P A and Whitehead J C 2011 *J. Phys. D: Appl. Phys.* **44** 274007

[34] Hales T C 2011 *Historical overview of the Kepler conjecture* (Springer) 65-82

[35] Falkenstein Z and Coogan J J 1997 *J. Phys. D: Appl. Phys.* 817-825

[36] Griffiths D J 2007 *Introduction to Electrodynamics, 3rd Edition* (Upper Saddle River: Prentice-Hall)

[37] Stuart M R 1955 *J. Appl. Phys.* **26** 1399

[38] Van Itterbeek A and De Clippeleir K 1947 *Physica* **13** 459-464

[39] Michels A, Sanders P and A. S 1935 *Physica* **2** 753-756

[40] Bryan A B 1929 *Phys. Rev.* **34** 615-617

[41] Wang L, Yi Y H, Zhao Y, Zhang R, Zhang J L and Guo H C 2015 *ACS Catal.* **5** 4167-4174

[42] Aerts R, Somers W and Bogaerts A 2015 *ChemSusChem* **8** 702-716

[43] Yi Y, Xu C, Wang L, Yu J, Zhu Q, Sun S, Tu X, Meng C, Zhang J and Guo H 2017 *Chem. Eng. J.* **313** 37-46

[44] Ramakers M, Michielsen I, Aerts R, Meynen V and Bogaerts A 2015 *Plasma Process. Polym.* **12** 755-763

[45] Sadeghi N, Setser D W and Touzeau M 2002 *J. Phys. Chem. A* **106** 8399-8405

[46] Taylor G W and Setser D W 1971 *Chem. Phys. Lett.* **8** 51-54

[47] Bogaerts A and Gijbels R 2000 *J. Anal. At. Spectrom.* **15** 441-449

[48] De Bie C, van Dijk J and Bogaerts A 2015 *The Journal of Physical Chemistry C* **119** 22331-22350

[49] Wang L, Liu S, Xu C and Tu X 2016 *Green Chemistry* **18** 5658-5666

[50] Lin S Y and Guo H 2004 *J. Phys. Chem. A* **108** 10066-10071

[51] Harding L B, Guadagnini R and Schatz G C 1993 *Journal of Physical Chemistry* **97** 5472-5481

[52] Arai H, Nagai S and Hatada M 1981 *Radiation Physics and Chemistry (1977)* **17** 211-216

[53] Friedrichs G, Herbon J T, Davidson D F and Hanson R K 2002 *Physical*

Chemistry Chemical Physics **4** 5778-5788

[54] Choe S-J, Kang H-J, Kim S-J, Park S-B, Park D-H and Huh D-S 2005 *Bulletin of the Korean Chemical Society* **26** 1682-1688

[55] Mills G A and Steffgen F W 1974 *Catalysis Reviews* **8** 159-210

[56] Li K, Yin C, Zheng Y, He F, Wang Y, Jiao M, Tang H and Wu Z 2016 *The Journal of Physical Chemistry C* **120** 23030-23043

[57] Butterworth T, Elder R and Allen R 2016 *Chem. Eng. J.* **293** 55-67

[58] Brand K P 1982 *IEEE Trans. Electr. Insul.* **EI-17** 451-456